

Study of temperature dependent atomic correlations in MgB₂

G. Campi¹, E. Cappelluti^{2,3}, Th. Proffen⁴, X. Qiu⁵, E. S. Bozin⁵, S. J. L. Billinge⁵, S. Agrestini³, N.L. Saini³, and A. Bianconi³

¹ Istituto di Cristallografia, CNR, sezione di Monterotondo, Area della Ricerca di Roma - Montelibretti, Po. Box 10, 00016 Monterotondo St.(RM), Italy

² Istituto dei Sistemi Complessi, CNR-INFM, v. dei Taurini 19, 00185 Roma, Italy

³ Dipartimento di Fisica, Università di Roma “La Sapienza”, P. le Aldo Moro 2, 00185 Roma, Italy

⁴ Lujan Neutron Scattering Center, Los Alamos National Laboratory, Los Alamos, New Mexico 87545, USA

⁵ Department of Physics and Astronomy, Michigan State University, East Lansing, Michigan 48824, USA

July 24, 2021/

Abstract. We have studied the evolution with temperature of the local as well as the average crystal structure of MgB₂ using the real-space atomic pair distribution function (PDF) measured by high resolution neutron powder diffraction. We have investigated the correlations of the B-B and B-Mg nearest neighbor pair motion by comparing, in the wide temperature range from $T = 10$ K up to $T = 600$ K, the mean-square displacements (MSD) of single atoms with the mean-square relative displacements (MSRD) obtained from the PDF peak linewidths. The results show that the single atom B and Mg vibrations are mostly decoupled from each other, with a small predominance of positive (in phase) correlation factor for both the B-B and B-Mg pairs. The small positive correlation is almost temperature independent, in contrast with our theoretical calculations; this can be a direct consequence of the strong decay processes of the E_{2g} anharmonic phonons.

PACS. 74.70.Ad Metals; alloys and binary compounds (including A15, MgB₂, etc.) – 61.12.-q Neutron diffraction and scattering – 63.20.-e Phonons in crystal lattices

1 Introduction

MgB₂ is the simplest system to investigate the quantum mechanism that allows the formation of a superconducting condensate with critical temperature $T_c \simeq 40$ K [1] a factor two higher than in all other known intermetallic superconductors. It was recently proposed by a few groups [2,4,3,5,6] that the enhancement of the critical temperature in MgB₂ is due to the exchange-like interband pairing in a multiband superconductor. There is now experimental evidence [7,8,9,10,11] that MgB₂ is the first clear case of a high T_c multiband superconductor showing two-gaps in the σ and π bands respectively, in agreement with the theory.[12,13]

The characteristic feature of MgB₂ is that the electron-phonon interaction gives a weak pairing in the π channel and a strong pairing in the σ -channel. Electronic band calculations,[14,15,16,17,18] Raman [16,19] and inelastic neutron scattering experiments [20] provide evidence of an extremely large deformation potential for the B bond stretching modes, which gives rise to strongly anharmonic phonons. This anharmonicity also results in a structural instability (phonon softening) that affects the dynamics of the lattice fluctuations and the local structural properties of the material, as we discuss below. There is now a general agreement that this strong electron-phonon cou-

pling is mainly driven by the interaction between electronic carriers in the 2D σ band with boron $p_{x,y}$ character and the zone center E_{2g} phonon mode.[12,13,14,15,16,17] This is reflected in a Kohn anomaly in the phonon dispersion related to the size of the small 2D tubular Fermi surfaces.[20] The proximity of the Fermi level to the Van Hove singularity (VHs) and to the band edge discloses a new scenario where the large amplitude of the expected boron zero point lattice fluctuations [7,12,15,18,21,22] induces large fluctuations of the same order of the separation between the VHs, the gap edge and the Fermi level itself. Although the amplitude of the lattice fluctuations seems thus to be highly relevant for the superconductivity in MgB₂ there is a lack of experimental information on this key point. Furthermore, although the average structure (P6/mmm) of the MgB₂ system has been exhaustively investigated, there is not yet any study of the local structure, since typical x-ray local probes, such as EXAFS, cannot be used to study local structure near light atoms.

In view of this, here we employ high resolution neutron diffraction to obtain the pair distribution function (PDF) of MgB₂. In this way we investigate the local as well as the average structure of MgB₂, namely the mean-square displacements (MSD) of single atoms and the mean-square relative displacements (MSRD). The comparison of these

quantities permits for the first time to extract the correlation factors $\rho_{\text{B-B}}$, $\rho_{\text{B-Mg}}$, defined below, of the boron-boron and boron-magnesium pair motions, which are found to be $\rho_{\text{B-B}} \sim 0.1$, $\rho_{\text{B-Mg}} \sim 0.1$, and nearly constant in a wide range of temperature $0 \text{ K} < T < 600 \text{ K}$. We also compare the experimental data with a constant force (CF) model for the phonon dispersion. We estimate that the phonon frequency renormalization due to the electron-phonon interaction on the E_{2g} modes yields a reduction $\Delta\rho_{\text{B-B}} \sim -0.03$ in the boron-boron correlation factor. While the CF model can nicely account for the zero temperature values of the single atoms MSD and the correlated MSRD, the temperature behavior of the correlation factor is shown to be highly anomalous and its physical interpretation gives rise to new questions about our understanding to the local lattice dynamics in this material.

2 Experimental method and data processing

Polycrystalline samples of MgB₂ were synthesized at high temperature by direct reaction of the elements in a tantalum crucible under argon atmosphere using pure ¹¹B isotopes. Time-of-flight neutron powder diffraction data were collected on the NPDF diffractometer at the Manuel Lujan, jr., Neutron Scattering Center (LANSCE) at Los Alamos National Laboratory. The NPDF diffractometer, with its high neutron flux and backscattering detector modules has a high resolution,[24] providing access to a wide range of momentum transfer with sufficient counting statistics making it ideal for PDF studies. The powdered samples were sealed inside extruded cylindrical vanadium containers. These were mounted on the stage of a cryofurnace with and without heat-shield for $T < 300 \text{ K}$ and $T > 300 \text{ K}$, respectively. The scattering data from the empty cryofurnace, with and without heat-shield, an empty container mounted on the cryofurnace, and the empty instrument were also collected, allowing us to assess and subtract instrumental backgrounds. The scattering from a vanadium rod was also measured to allow the data to be normalized for the incident spectrum and detector efficiencies. We collected each diffraction spectrum up to the high momentum transfer of $Q = 40 \text{ \AA}^{-1}$ in 3 hours. The high resolution diffraction spectrum so obtained presents both the Bragg peaks and the diffuse scattering. While the Bragg peaks reflect the long-range order of the crystalline samples, the oscillating diffuse scattering contains local structural information including the correlated dynamics.[29,31] The PDF is obtained from a Fourier transform of the powder diffraction spectrum (Bragg peaks + diffuse scattering).[23] It consists of a series of peaks, the positions of which give the distances of atom pairs in the real space, while the ideal width of these peaks is due both to relative thermal atomic motion and to static disorder. This permits the study of the effects of lattice fluctuations on PDF peak widths and yields information on both the single atom mean-square displacements and the relative mean-square displacements of atom pairs and their correlations.

Standard data corrections [23] were carried out using the program PDFGETN.[25] After being corrected, the data were normalized by the total scattering cross section of the sample to yield the total scattering structure function $S(Q)$. Afterwards, the total scattering structure function $S(Q)$ is converted to the PDF, $G(r)$, by means of a sine Fourier transform according to the relation:

$$\begin{aligned} G(r) &= 4\pi r(\rho(r) - \rho_0) \\ &= \frac{2}{\pi} \int_0^\infty Q[S(Q) - 1] \sin(Qr) dQ. \end{aligned} \quad (1)$$

We modeled the PDF using a structural model that takes advantage of the definition of the radial distribution function RDF $R(r)$, namely:

$$R(r) = rG(r) + 4\pi r^2 \rho_0 = \sum_{i \neq j} \frac{b_i b_j}{\langle b \rangle^2} \delta(r - r_{ij}), \quad (2)$$

where b_i is the scattering length of the i^{th} atom, $\langle b \rangle$ is the scattering length averaged over the sample composition, $r_{ij} = |\mathbf{r}_i - \mathbf{r}_j|$ is the distance between the i^{th} and the j^{th} atoms, and the sums are taken over all the atoms in the sample. Before being compared to the data, the calculated $G(r)$ is convoluted with a termination function, $\sin(Q_{\text{max}}r)/r$ to account for the effects of the finite data collection range. Fundamental lattice information, such as the average crystal structure, the lattice constants, a scale factor, and the refined atomic (thermal) displacement parameters, can now be extracted from the PDF by using the PDF refinement program PDFFIT [26] that is based on a least-squares approach to fit the PDF profile. The average atomic displacement distribution of atom i along the major axes x , y , and z , $\sigma^2(i_x)$, $\sigma^2(i_y)$, $\sigma^2(i_z)$, are defined as

$$\sigma^2(i_\alpha) = \langle [\mathbf{u}_i \cdot \hat{\mathbf{r}}_\alpha]^2 \rangle, \quad (3)$$

where \mathbf{u}_i is the lattice displacement of atom i from its average position [27] and $\hat{\mathbf{r}}_\alpha$ is the unit vector pointing along the direction $\alpha = x, y, z$. Due to the geometry of these compounds, the two boron atoms for the unit cell are equivalent and $\sigma^2(i_x) = \sigma^2(i_y)$ for all the atoms, so that only four parameters were needed namely $\sigma^2(\text{B}_{xy})$, $\sigma^2(\text{B}_z)$, $\sigma^2(\text{Mg}_{xy})$ and $\sigma^2(\text{Mg}_z)$.

3 Results and discussion

In Fig. 1 we show the reduced scattering structure function $Q[S(Q) - 1]$ for the MgB₂ at $T = 300 \text{ K}$, while the corresponding reduced PDF, $G(r)$, obtained using Eq. (1), is shown in Fig. 2. The features of the NPDF diffractometer allowed us to obtain high quality PDFs as can be noted by inspecting the modeled fit (solid line) of the $G(r)$ in the upper panel Fig. 2. This can be seen also in the lower panel of Fig. 2 where most of the fluctuations in the difference curve (solid line) are within the standard deviation on the data $\pm \Delta[G(r)]$ (dashed lines above and below the difference curve).

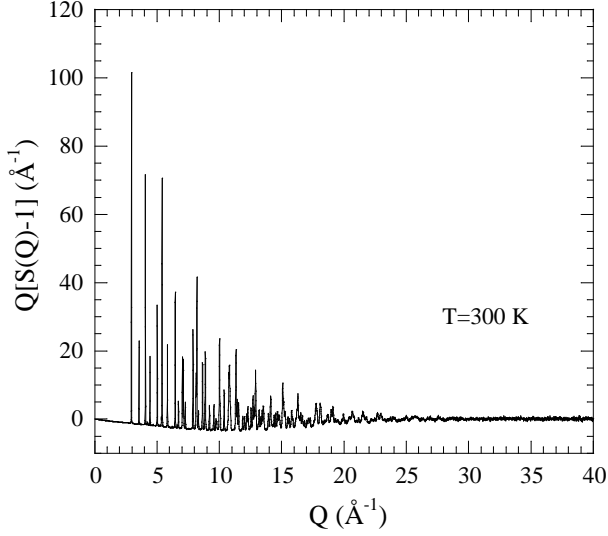


Fig. 1. The reduced structure function $Q[S(Q) - 1]$ for MgB₂ measured at 300 K.

The PDF's have been fit over the range 1–18 Å using a hexagonal crystal structure (space group P6/mmm), and excellent fits were obtained at all temperatures. The Bragg peaks are clearly persistent up to 25 Å⁻¹, reflecting both the long-range order of the crystalline samples and the small amount of positional (vibrational or static) disorder of the atoms around their average positions.

The lattice parameters at $T = 300$ K for MgB₂ ($T_c \sim 39$ K) were found to be $a = 3.08505(4)$ Å, $c = 3.5218(1)$ Å. The lattice displacements $\sigma^2(B_{xy})$, $\sigma^2(B_z)$, $\sigma^2(Mg_{xy})$, $\sigma^2(Mg_z)$ are shown in Fig. 3 (open circles).

3.1 Atomic mean-square displacements

In order to extract information about the phonon spectrum, we fit each lattice displacement with a simple Einstein model,

$$\sigma^2(i_\alpha) = \frac{\hbar}{M_i \omega_{i_\alpha}} \left[\frac{1}{2} + n[\omega(i_\alpha)] \right] + \sigma_0^2(i_\alpha), \quad (4)$$

where $\sigma_0^2(i_\alpha)$ takes into account the static disorder, M_i is atomic mass of the atom i and $\omega(i_\alpha)$ provided an estimate of the vibrational frequency of the atom i along the direction α . The quantity $n(x)$ is the Bose thermal factor $n[x] = [\exp(x/k_B T) - 1]^{-1}$. The values of the fitting parameters, ω_{i_α} and $\sigma_0^2(i_\alpha)$, are reported in Tab. 1, and the σ^2 vs. T fitting curves are represented by dotted lines in Fig. 3. The different values of ω_{i_α} represent the different energy range of the phonon spectra associated with the boron and magnesium in-plane and out-of-plane lattice vibrations, and they are in good agreement with the corresponding spectra reported in Ref. [28].

Quite surprising, we find that, apart from some amount of disorder in $\sigma_0^2(Mg_z)$, this simple four-peak Einstein model seems to describe quite well the lattice vibrations in this compound. This is quite intriguing because phonon

frequency dispersions are expected to be notably different from dispersionless Einstein models in these materials. Moreover, the Einstein fits were obtained by simply using an effective atomic mass $M_{Mg} = 24.3$ a.m.u. for $\sigma^2(Mg)$ and $M_B = 10.81$ a.m.u. for $\sigma^2(B)$. This means that we are implicitly assuming that magnesium and boron vibrations are totally decoupled from each other. These two-parameter fits reproduce the data very well for each of the motions considered. Non-independent boron and magnesium vibrations would lead to deviations from Einstein behavior that are not evident in the data suggesting that this approximation is reasonable in this system. We return to this point below.

To gain further insight on this issue we introduce a constant force (CF) shell model for the dynamical matrix. We neglect for the moment the effects of the electron-phonon interaction, which leads to renormalized phonon frequencies and anharmonicity, and we assume the lattice

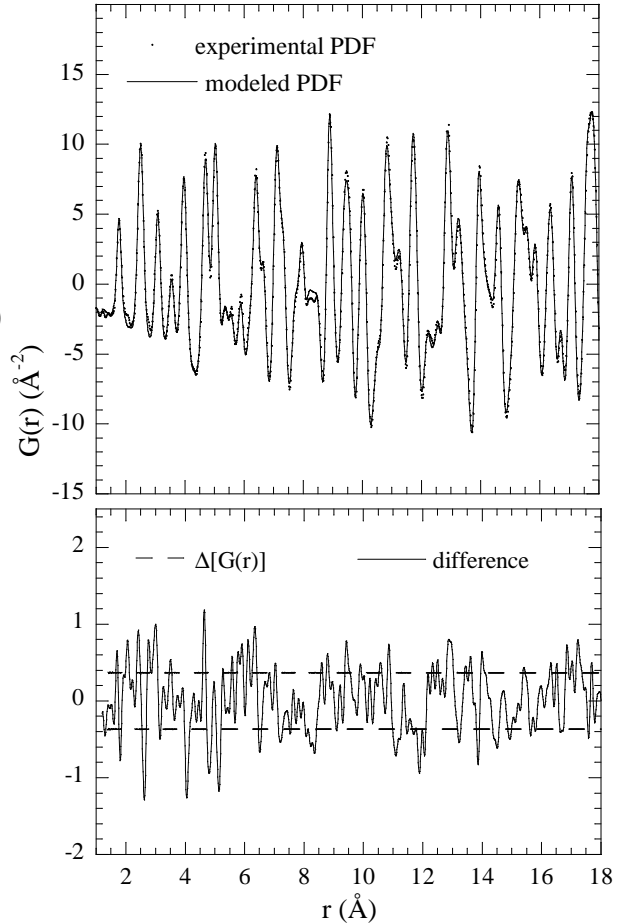


Fig. 2. (Upper panel) The PDF $G(r) = 4\pi r[\rho(r) - \rho_0]$, obtained from Eq. 1 for MgB₂, measured at 300 K (dots), with the structure refinement curve obtained by a least-squares approach (solid line). (Lower panel) The difference curve (solid line) of the experimental PDF with the modeled fit and the standard deviation on the data $\pm\Delta[G(r)]$ (dashed lines) are shown. We can observe that most of the fluctuations in the difference curve are within $\pm\Delta[G(r)]$.

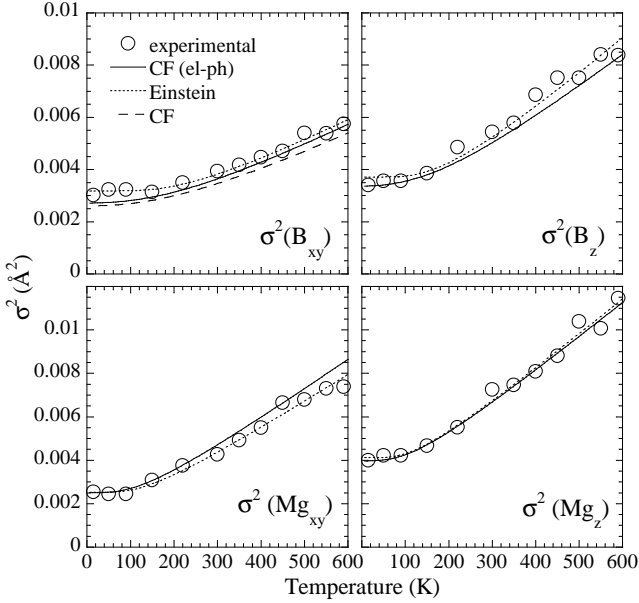


Fig. 3. Anisotropic in plane $\sigma^2(B_{xy})$, $\sigma^2(Mg_{xy})$ and along the c-axis $\sigma^2(B_z)$, $\sigma^2(Mg_z)$ mean-square displacements for the B and Mg atoms, as a function of the temperature. The open circles represent the PDFFIT refined values, while the solid and the dotted lines represent the modeled data in the CF and Einstein model, respectively. The errorbars in the $\sigma^2(i_\alpha)$ are smaller than the size of the used symbols (open circles). The dashed line shows the in-plane boron lattice displacements in the CF model in the absence of the electron-phonon interaction.

$\omega(B_{xy})$ (K)	703 ± 10
$\omega(B_z)$ (K)	572 ± 15
$\omega(Mg_{xy})$ (K)	398 ± 6
$\omega(Mg_z)$ (K)	350 ± 9
$\sigma_0^2(B_{xy})$ (\AA^2)	$\leq 5 \cdot 10^{-5}$
$\sigma_0^2(B_z)$ (\AA^2)	$\leq 9 \cdot 10^{-5}$
$\sigma_0^2(Mg_{xy})$ (\AA^2)	$\leq 7 \cdot 10^{-5}$
$\sigma_0^2(Mg_z)$ (\AA^2)	0.0013 ± 0.0003

Table 1. “Effective” phonon frequencies ω_{i_α} and static disorder contributions $\sigma_0^2(i_\alpha)$ for the in-plane and out-of-plane B and Mg displacements as obtained by the Einstein model fit [Eq. (4)] of $\sigma^2(i_\alpha)$.

dynamics to be harmonic (we shall discuss later and more specifically the role of the electron-phonon interaction and possible effects of the anharmonicity of the E_{2g} phonon mode). This will enable us to evaluate eigenvectors $\hat{\epsilon}_{\mathbf{q},\mu}$ and eigenvalues $\omega_{\mathbf{q},\mu}$ of the lattice modes for each point of the phonon Brillouin zone. The phonon contribution to the lattice displacements $\sigma^2(i_\alpha)$ [$\sigma^2(i_\alpha) = \sigma_{\text{ph}}^2(i_\alpha) + \sigma_0^2(i_\alpha)$] will be thus obtained as:[33]

$$\sigma_{\text{ph}}^2(i_\alpha) = \frac{\hbar}{N} \sum_{\mathbf{q},\mu} \frac{|\epsilon_{\mathbf{q},\mu}^{i_\alpha}|^2}{M_i \omega_{\mathbf{q},\mu}} \left[\frac{1}{2} + n(\omega_{\mathbf{q},\mu}) \right], \quad (5)$$

ϕ_r (eV/ \AA^2)	ϕ_{\parallel} (eV/ \AA^2)	ϕ_{\perp} (eV/ \AA^2)
12,45	49.80	21.17
χ_r (eV/ \AA^2)	χ_{\parallel} (eV/ \AA^2)	χ_{\perp} (eV/ \AA^2)
0.0	16.6	0.0
κ_r (eV/ \AA^2)	κ_{\parallel} (eV/ \AA^2)	κ_{\perp} (eV/ \AA^2)
0.84	1.50	9.14
ψ_r (eV/ \AA^2)	ψ_{\parallel} (eV/ \AA^2)	ψ_{\perp} (eV/ \AA^2)
0.0	9.34	0.42

Table 2. Force constant parameters reproducing the bare phonon dispersion in MgB₂ in the absence of electron-phonon interaction.

where $\epsilon_{\mathbf{q},\mu}^{i_\alpha}$ is the component of the eigenvector $\hat{\epsilon}_{\mathbf{q},\mu}$ concerning to the displacement of the i atom along the α direction and N is the total number of \mathbf{q} -points considered in the phonon Brillouin zone. From a general point of view, since $\sigma_{\text{ph}}^2(i_\alpha)$ involves an integral over the whole Brillouin zone and over all the phonon branches, it will not be sensitive to the fine details of the phonon dispersion but only to its gross features. For this reason, and in order to preserve the simplicity of our analysis, we limit ourselves to consider only four elastic springs, ϕ , χ , κ and ψ , connecting, respectively, in-plane B-B nearest neighbors, out of plane B-B nearest neighbors, out-of-plane B-Mg nearest neighbors, and in-plane Mg-Mg nearest neighbors. Each elastic spring is specified by its tensor components (ex.: ϕ_r , ϕ_{\parallel} , ϕ_{\perp}), corresponding respectively to the lattice displacements along the radial (bond-stretching) direction and along the in-plane and out-of-plane tangential (bond-bending) directions. In MgB₂ we choose the constants ϕ_r , ϕ_{\parallel} , ϕ_{\perp} , χ_r , χ_{\parallel} , χ_{\perp} , κ_r , κ_{\parallel} , κ_{\perp} , ψ_r , ψ_{\parallel} , ψ_{\perp} , to fit the local-density functional (LDA) phonon dispersion of Ref. [16] along the high-symmetry points of the Brillouin zone. Since the constant force model is meant to reproduce the bare phonon dispersion, we deliberately did not include in the fit procedure the E_{2g} phonon frequencies at the zone center Γ , A , which are known to be strongly affected by the el-ph interaction. The elastic constants obtained from this fitting procedure are reported in Table 2.

As mentioned in the introduction, the E_{2g} phonon modes close to the Γ and A points are expected to be strongly affected by the interaction with the almost 2D parabolic σ bands, giving rise to a remarkable softening of the E_{2g} phonon frequencies for $|\mathbf{q}| \leq 2k_F$, where k_F is the Fermi vector of the σ bands.[14,15,16,17,20] We include these effects through the self-energy renormalization of the phonon frequencies $\Omega_{E_{2g}}^2(\mathbf{q}) = \omega_{E_{2g}}^2(\mathbf{q}) - (4N_\sigma g^2 f_{\text{anharm}}/M_B) \Pi_{2D}(\mathbf{q})$, where N_σ is density of states of the σ bands per spin and per band, g the electron-phonon matrix element between σ -band electrons and the E_{2g} phonon mode at the zone center and f_{anharm} is a dimensionless factor accounting for the anharmonic hardening of the E_{2g} phonon modes due to the electron-phonon coupling itself. Moreover the factor 4 takes into account the spin and band degeneracy and $\Pi_{2D}(\mathbf{q})$ is the two-dimensional Lindhardt function $\Pi_{2D}(x) = \theta(1-x) + \theta(x-1)[x - \sqrt{x^2 - 1}]/x^4$, with $x = |\mathbf{q}|/2k_F$. We take, from first-principle calculations,[14,15,18] $f_{\text{anharm}} = 1.25$, $N_\sigma = 0.075$ states/(eV · spin · cell) $g = 12$

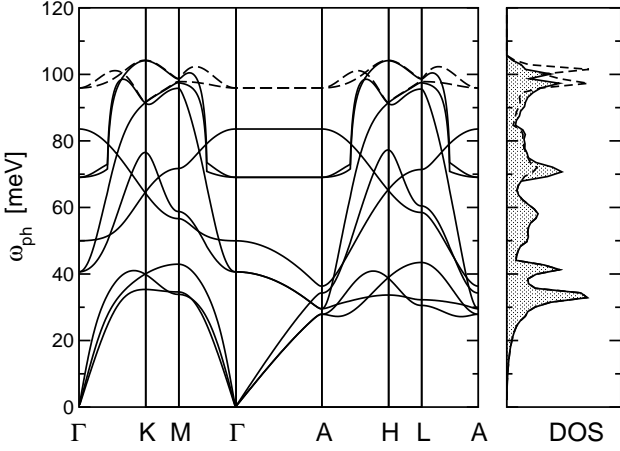


Fig. 4. Phonon dispersion and phonon density of states for MgB₂ evaluated within the CF model. Dashed lines represent the same quantities without taking into account the electron-phonon interaction.

$\text{eV}/\text{\AA}$ and $k_F \simeq \pi/12d_{\text{B-B}}$, where $d_{\text{B-B}}$ is the boron-boron distance.

The phonon dispersion and phonon density of states (PDOS) of our constant force model are shown in Fig. 4, in good agreement with the LDA calculations of Ref. [16]. For comparison, the dashed lines represent the bare phonon dispersion in the absence of el-ph interaction and the corresponding PDOS. Most striking is a partial shift in spectral weight from 100 meV to 70 meV when the el-ph coupling is turned on, due to the softening of the flat $\Gamma - A$ band originating from the E_{2g} phonons.

The lattice displacements for each atom and for each direction can now be evaluated directly by means of Eq. (5). The results are also shown in Fig. 3 along with the data extracted by the PDF analysis and with the simple Einstein fits. In spite of the crude simplification of the phonon dispersion, the agreement with the PDF data is remarkable. Just as in the Einstein fits, we find that a constant shift $\sigma_0^2(\text{Mg}_z) \simeq 0.0013 \text{ \AA}^2$ due to intrinsic disorder is needed to account for the magnesium out-of-plane lattice vibration while the contribution of the disorder for the other modes is found to be negligible. Note that the agreement between the data and solid lines was obtained with *no adjustable parameters*. The values used in the constant force models in Table 2 were indeed fit to reproduce the theoretical LDA calculation and not the PDF data and the only other parameter, the static disorder parameter in $\sigma_0^2(\text{Mg}_z)$, was the same value as was used in the Einstein fits. The agreement with the data and the Einstein model fits is also very good suggesting that boron and magnesium lattice vibrations, as well as in-plane and out-of-plane lattice vibrations, are on average independent each other.

To point out the explicit role of the electron-phonon interaction, we show also in the left-upper panel of Fig. 3 the $\sigma_0^2(\text{B}_{xy})$ lattice displacements in the absence of the el-ph frequency renormalization. Since only E_{2g} phonons are coupled, only the $\sigma_0^2(\text{B}_{xy})$ lattice displacements result modified. We note that the inclusion of electron-phonon interaction effects leads to a slight increase of the amount

of the boron in-plane lattice displacements, with a better agreement with the experimental data. The increase of $\sigma_0^2(\text{B}_{xy})$ is easily understandable as due to the softening of the E_{2g} phonon mode. On the other hand, since the electron-phonon renormalization effects are restricted to a small region $\sqrt{q_x^2 + q_y^2} \leq 2k_F$ of the whole Brillouin zone, the impact of the el-ph coupling on the total amount of the lattice displacements $\sigma_0^2(\text{B}_{xy})$ is relatively weak. As we are going to see, the effects of the electron-phonon interaction are more apparent in the correlated pair motion.

3.2 Correlations in the B-B and B-Mg atomic pairs motion

Above we showed that the average uncorrelated thermal motions (equivalent to the Debye-Waller factor in crystallography) measured from MgB₂ are well explained by harmonic models with independent boron and magnesium motions. A strength of the PDF technique is that it is sensitive to correlations in the atomic dynamics that contain some additional details about the underlying interatomic potentials.[27,29,30,31] Here we explore the motional correlations in the MgB₂ PDF data.

The Gaussian width σ_{ij} of the PDF peaks is directly related to the mean-square relative displacement of atomic pairs projected onto the vector joining the atom pairs.[27] Explicitly,

$$\sigma_{ij}^2 = \langle [(\mathbf{u}_i - \mathbf{u}_j) \cdot \hat{\mathbf{r}}_{ij}]^2 \rangle, \quad (6)$$

where \mathbf{u}_i and \mathbf{u}_j are the lattice displacements of atoms i and j from their average positions, $\hat{\mathbf{r}}_{ij}$ is the unit vector connecting atoms i and j , and where the angular brackets indicate an ensemble average.[27]

In our analysis, we focus on the width of the nearest neighbor boron-boron PDF peak, ($\sigma_{\text{B-B}}^2$), and on the nearest neighbor magnesium-boron peak, ($\sigma_{\text{B-Mg}}^2$). These are well resolved single-component peaks in the PDF whose width directly yields correlated dynamical information. [31] The Gaussian widths $\sigma_{\text{B-B}}^2$, $\sigma_{\text{B-Mg}}^2$, as measured by the PDF data are shown in the upper panels of Fig. 5 (open circles) along with the same quantity evaluated within the CF model (solid line) according to the relation:

$$\sigma_{ij}^2 = \frac{\hbar}{N} \sum_{\mathbf{q}, \mu} \left[\frac{1}{2} + n(\omega_{\mathbf{q}, \mu}) \right] \left\{ \frac{|\hat{\mathbf{e}}_{\mathbf{q}, \mu}^i \cdot \hat{\mathbf{r}}_{ij}|^2}{M_i \omega_{\mathbf{q}, \mu}} + \frac{|\hat{\mathbf{e}}_{\mathbf{q}, \mu}^j \cdot \hat{\mathbf{r}}_{ij}|^2}{M_j \omega_{\mathbf{q}, \mu}} - \frac{2\text{Re} \left[(\hat{\mathbf{e}}_{\mathbf{q}, \mu}^i \cdot \hat{\mathbf{r}}_{ij}) (\hat{\mathbf{e}}_{\mathbf{q}, \mu}^{j*} \cdot \hat{\mathbf{r}}_{ij}) e^{i\mathbf{q} \cdot \mathbf{r}_{ij}} \right]}{\omega_{\mathbf{q}, \mu} \sqrt{M_i M_j}} \right\}. \quad (7)$$

In this latter case in the right panel for $\sigma_{\text{B-Mg}}^2$ we have also added a small contribution of the local lattice displacements due to the disorder (see below for more details).

Here we first note that, while the zero temperature values of $\sigma_{\text{B-B}}^2$, $\sigma_{\text{B-Mg}}^2$ are well reproduced by the CF model, this model is less good than was the case for the uncorrelated motions, especially at high temperatures.

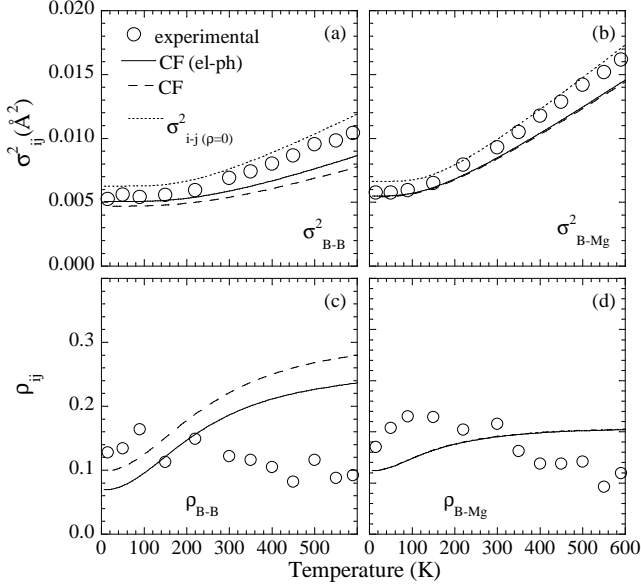


Fig. 5. Mean-square relative lattice displacements σ_{B-B}^2 (a), σ_{B-Mg}^2 (b), as extracted from the width of the PDF peaks and the corresponding correlation function ρ_{B-B} (c), ρ_{B-Mg} (d) (open circles). Solid lines represent the same quantities evaluated within the CF model, while dotted lines in the upper panels show the predicted relative lattice displacements σ_{B-B}^2 , σ_{B-Mg}^2 for completely uncorrelated lattice motion $\rho_{B-B} = 0$, $\rho_{B-Mg} = 0$. The dashed lines in the upper panels represent the relative lattice displacement σ_{B-B}^2 and σ_{B-Mg}^2 evaluated within the CF model in the absence of the electron-phonon interaction.

The temperature dependence of the single-atom motions was well explained by the model, but not those of the correlated σ_{ij}^2 , which suggests that the model is not capturing some aspect of the motional correlations. Introducing the electron-phonon coupling into the model improves the agreement slightly, with a larger effect observed on σ_{B-B}^2 , but this does not explain all of the discrepancy. In each case, the pair correlation peaks broaden more quickly in the data than in the model. We note that the models are harmonic. Even in the case where we have introduced electron-phonon coupling, harmonic spring constants have been obtained from a fit to the LDA bands and we speculate that the discrepancy at high temperature is a result of anharmonicity in the boron motion.

As a general consideration, we would like to stress once more that while $\sigma^2(i_\alpha)$ probes the absolute magnitude of the single atom mean-square displacement, σ_{ij}^2 provides information about the *correlation* between the lattice displacements of atom pairs. Let us consider for instance the case of σ_{B-B}^2 which involves only boron in-plane lattice fluctuations. We can identify three limiting behaviors for this quantity: *i*) perfectly in-phase lattice motion; *ii*) perfectly opposite-phase motion; *iii*) completely independent motion. In the first case it is easy to see that $\sigma_{B-B}^2 = 0$, while $\sigma_{B-B}^2 = 2\sigma^2(B_{xy})$ when the nearest neighbor boron lattice displacements are uncorrelated, and $\sigma_{B-B}^2 = 4\sigma^2(B_{xy})$ when they have opposite phase.

To formalize this we rearrange Eq. (6) as

$$\sigma_{ij}^2 = \langle [(\mathbf{u}_i \cdot \hat{\mathbf{r}}_{ij})^2] \rangle + \langle [(\mathbf{u}_j \cdot \hat{\mathbf{r}}_{ij})^2] \rangle - 2\langle (\mathbf{u}_i \cdot \hat{\mathbf{r}}_{ij}) \cdot (\mathbf{u}_j \cdot \hat{\mathbf{r}}_{ij}) \rangle. \quad (8)$$

Here the first two terms are related to mean-square thermal displacement of atoms i and j projected along $\hat{\mathbf{r}}_{ij}$, while the third term is a displacement correlation function, which carries information about the motional correlations. It is now useful to quantify the degree of correlation by introducing the dimensionless correlation parameter ρ_{ij} defined as: [33,29,31,32]

$$\sigma_{ij}^2 = \sigma^2(i_j) + \sigma^2(j_i) - 2\sigma(i_j)\sigma(j_i)\rho_{ij}, \quad (9)$$

where $\sigma^2(i_j) = \langle [(\mathbf{u}_i \cdot \hat{\mathbf{r}}_{ij})^2] \rangle$. Positive values of $\rho > 0$ describe a situation where the atoms move in phase, so that the resulting value of σ_{ij}^2 is smaller than for the uncorrelated case. On the other hand, a predominance of opposite phase atomic vibrations should result in $\rho < 0$ and in a PDF peak width σ_{ij}^2 larger than the uncorrelated case.

It is important to note that the correlation function ρ_{ij} in Eq. (9) expresses the degree of correlation between the *total* atomic displacements. In the presence of two different sources of lattice displacements (phonons and disorder), it is more convenient to split σ_{ij}^2 into a phonon and a disorder contribution. Assuming the local lattice displacements due to the disorder to be uncorrelated, we can write thus:

$$\sigma_{ij}^2 = \sigma_{\text{ph}}^2(i_j) + \sigma_{\text{ph}}^2(j_i) - 2\sigma_{\text{ph}}(i_j)\sigma_{\text{ph}}(j_i)\rho_{ij} + \sigma_0^2(i_j) + \sigma_0^2(j_i), \quad (10)$$

where ρ_{ij} represents now only the correlation between *phononic* lattice displacements.

Using Eq. (10) the correlation parameter can be calculated from the total width of the PDF peak as

$$\rho_{ij} = \frac{\sigma_{\text{ph}}^2(i_j) + \sigma_{\text{ph}}^2(j_i) + \sigma_0^2(i_j) + \sigma_0^2(j_i) - \sigma_{ij}^2}{2\sigma_{\text{ph}}(i_j)\sigma_{\text{ph}}(j_i)}. \quad (11)$$

Finally, the projected atomic mean-square displacements $\sigma^2(i_j)$ (lattice vibrations along the pair $\hat{\mathbf{r}}_{ij}$ direction) can be related to $\sigma_{i_\alpha}^2$ (lattice vibrations along the Cartesian axes) by simple geometrical considerations. We have thus $\sigma_{\text{ph}}^2(B_B) = \sigma_{\text{ph}}^2(B_{xy})$, $\sigma_{\text{ph}}^2(B_{Mg}) = [4R^2\sigma_{\text{ph}}^2(B_{xy}) + 3\sigma_{\text{ph}}^2(B_z)]/(4R^2 + 3)$, $\sigma_{\text{ph}}^2(Mg_B) = [4R^2\sigma_{\text{ph}}^2(Mg_{xy}) + 3\sigma_{\text{ph}}^2(Mg_z)]/(4R^2 + 3)$, where $R = a/c = 0.88$ and where a and c are the in-plane and out-of-plane lattice constants. Similar relations hold true for the disorder contributions.

The phonon correlation factor ρ_{ij} as extracted from the PDF data σ_{B-B}^2 , σ_{B-Mg}^2 , and from the single atom mean-square lattice displacements $\sigma^2(i_\alpha)$ is shown in the lower panels of Fig. 5 (open circles), together with the corresponding correlation factor predicted by the CF model (solid lines). In order to extract the experimental value of ρ_{B-Mg} we have taken into account a slight magnesium disorder along the c axis, $\sigma_0^2(Mg_z) = 0.0013 \text{ \AA}^2$, in agreement with the previous analysis of the mean square absolute displacements $\sigma^2(i_\alpha)$. We find a positive correlation factor for both $\rho_{B-B} \sim 0.1$ and $\rho_{B-Mg} \sim 0.1$, indicating a

slight predominance of the in-phase B-B and B-Mg lattice displacements in this experimental probe. Positive values of ρ_{ij} are commonly reported in a variety of materials. The intuitive explanation is that the in-phase phonon modes (acoustic, low optical branch modes) are generally less stiff than the opposite-phase optical ones. Our reported values of $\rho_{B-B}, \rho_{B-Mg} \sim 0.1$ are however much smaller than the correlation factors commonly found in other covalently bonded materials.[33,29,31,32] This observation points out once more that all the motions are decoupled and the atoms are behaving largely like independent oscillators.

Another anomalous feature of MgB₂ pointed out by this analysis is the lack of a temperature dependence for the correlation factors ρ_{ij} as compared with the CF model and with the standard behavior of other common materials.[31] An increase of ρ_{ij} as function of temperature is indeed observed in many covalently bonded systems and it is essentially due to the fact that the thermal population of the low frequency in-phase phonon modes is larger than the high frequency out-of-phase phonon modes. The lack of this temperature dependence in our measurements can maybe be attributed to the anharmonic character of the high frequency (E_{2g}) B-B modes and it represents an interesting anomaly in this material whose physical interpretation can shed interesting light on the lattice dynamics in MgB₂. Further work on this subject is required. As a final point, we can quantify in our model the role of the electron-phonon coupling on the correlation factors. As shown in Fig. 5 the inclusion of the electron-phonon interaction, which leads to a partial softening of the out-of-phase E_{2g} in-plane boron displacements, is reflected in a significant reduction $\Delta\rho_{B-B} \sim -0.03$ of the correlation factor ρ_{B-B} while a negligible effect is found on ρ_{B-Mg} .

4 Conclusions

In this work we have investigated the local lattice properties of MgB₂ paying special attention on the lattice dynamics and the correlations in the B-B and B-Mg first neighbor atomic pair motion. We have used the real space PDF obtained from high resolution neutron diffraction to study the effects of the lattice vibrations on the PDF peak widths. The PDF peaks in well ordered crystals such as the present case yield important information about the underlying atomic potentials through the correlated local lattice dynamics. The data have been modeled using both a multi-parameter constant force model and a simple Einstein model. We have found that the constant force model as well as the Einstein one reproduce the average features of the lattice vibrations. This agreement suggests that boron and magnesium displacements, both in-plane and out-of-plane, are mostly independent of each other. The analysis of the PDF peak linewidths permits to evaluate the correlation for both the nearest neighbor B-B and B-Mg atomic pairs. We find a small positive correlation factor $\rho_{B-B} \sim 0.1$ and $\rho_{B-Mg} \sim 0.1$, nearly temperature independent, indicating a weakly prevalent in-phase relative atomic motion. These results are in contrast with CF

model which predicts correlation factors increasing with the temperature. This discrepancy supports the idea that anharmonic effects and strong decay processes for the E_{2g} B bond stretching modes are present, presumably due to the strong electron-phonon coupling.

Acknowledgements

This work is supported by MIUR in the frame of the project Cofin 2003 “Leghe e composti intermetallici: stabilità termodinamica, proprietà fisiche e reattività” on the “synthesis and properties of new borides” and by European project 517039 “Controlling Mesoscopic Phase Separation” (COMEPHS) (2005). E.C. acknowledges in addition funding from the FIRB project RBAU017S8R of MIUR. Work in the Billinge-group is supported by NSF through grant DMR-0304391. The NPDF diffractometer at the Lujan Center, Los Alamos National Laboratory, was funded by DOE through contract W-7405-ENG-36.

References

1. J. Nagamatsu, N. Nakagawa, T. Muranaka, Y. Zenitali, and J. Akimitsu, *Nature* **410**, 63 (2001).
2. S. Agrestini, D. Di Castro, M. Sansone, N. L. Saini, A. Saccone, S. De Negri, M. Giovannini, M. Colapietro, and A. Bianconi, *J. of Phys.: Cond. Matter* **13**, 11689 (2001).
3. A. Bianconi, D. Di Castro, S. Agrestini, G. Campi, N.L. Saini, A. Saccone, S. De Negri, and M. Giovannini, *J. Phys.: Condens. Matter* **13**, 7383 (2001).
4. M. Imada, *J. Phys. Soc. Jpn.* **70**, 1218 (2001).
5. K. Yamaji, *J. Phys. Soc. Jpn.* **70**, 1476 (2001).
6. T. Örd and N. Kristoffel, *Physica C* **370**, 17 (2002).
7. F. Bouquet, R.A. Fisher, N.E. Phillips, D.G. Hinks, and J.D. Jorgensen, *Phys. Rev. Lett.* **87**, 047001 (2001).
8. P. Szabo, P. Samuely, J. Kacmarcik, Th. Klein, J. Marcus, D. Fruchart, S. Miraglia, C. Marcenat, and A.G.M. Jansen, *Phys. Rev. Lett* **87**, 137005 (2001).
9. F. Giubileo, D. Roditchev, M. Sacks, R. Lassey, D.X. Thanh, and J. Klein, *Phys. Rev. Lett.* **87**, 177008 (2001).
10. S. Tsuda, T. Yokoya, Y. Takano, H. Kito, A. Matsushita, F. Yin, J. Itoh, H. Harima, and S. Shin, *Phys. Rev. Lett.* **91**, 127001 (2003).
11. R.S. Gonnelli, D. Daghero, G.A. Ummarino, V.A. Stepanov, J. Jun, S.M. Kazakov, and J. Karpinski, *Phys. Rev. Lett.* **89**, 247004 (2003).
12. A.Y. Liu, I.I. Mazin, and J. Kortus, *Phys. Rev. Lett* **87**, 087005 (2001).
13. H.J. Choi, D. Roundy, H. Sun, M.L. Cohen, and S.G. Louie, *Phys. Rev. B* **66**, 020513 (2002); *ibid.* *Nature*, **418**, 758 (2002).
14. J.M. An and W.E. Pickett, *Phys. Rev. Lett.* **86**, 4366 (2001).
15. T. Yildirim, O. Gülseren, J.W. Lynn, C.M. Brown, T.J. Udovic, Q. Huang, N. Rogado, K.A. Regan, M.A. Hayward, J.S. Slusky, T. He, M.K. Haas, P. Khalifah, K. Inumaru, and R.J. Cava, *Phys. Rev. Lett.* **87**, 037001 (2001).
16. K.-P. Bohnen, R. Heid, and B. Renker, *Phys. Rev. Lett.* **86**, 5771 (2001).

17. Y. Kong, O.V. Dolgov, O. Jepsen, and O.K. Andersen, Phys. Rev. B **64**, 020501 (2001).
18. L. Boeri, G.B. Bachelet, E. Cappelluti, and L. Pietronero, Phys. Rev. B **65**, 214501 (2002).
19. D. Di Castro, S. Agrestini, G. Campi, A. Cassetta, M. Colapietro, A. Congeduti, A. Continenza, S. De Negri, M. Giovannini, S. Massidda, M. Nardone, A. Pifferi, P. Postorino, G. Profeta, A. Saccone, N. L. Saini, G. Satta, and A. Bianconi, Europhys.Lett. **58**, 278 (2002).
20. A. Shukla, M. Calandra, M. d'Astuto, M. Lazzeri, F. Mauri, C. Bellin, M. Krisch, J. Karpinski, S.M. Kazakov, J. Jun, D. Daghero, and K. Parlinski, Phys. Rev. Lett. **90**, 095506 (2003).
21. A. Bianconi, S. Agrestini, D. Di Castro, G. Campi, G. Zangari, N.L. Saini, A. Saccone, S. De Negri, M. Giovannini, G. Profeta, A. Continenza, G. Satta, S. Massidda, A. Cassetta, A. Pifferi and M. Colapietro, Phys. Rev. B **65**, 174515 (2002).
22. L. Boeri, E. Cappelluti, and L. Pietronero, Phys. Rev. B **71**, 012501 (2005).
23. T. Egami and S.J.L. Billinge, *Underneath the Bragg peaks: structural analysis of complex materials* (Pergamon Press, Oxford, 2003).
24. Th. Proffen, T. Egami, S.J.L. Billinge, A.K. Cheetham, D. Louca and J.B. Parise, Appl. Phys. A-Mater. Sci. Process. **74**, S163 (2002)
25. P.F. Peterson, M. Gutmann, Th. Proffen, and S.J.L. Billinge, J. Appl. Crystallogr. **33**, 1192 (2000).
26. Th. Proffen and S.J.L. Billinge, J. Appl. Crystallogr. **32**, 572 (1999).
27. M. F. Thorpe, V. A. Levashov, M. Lei and S. J. L. Billinge, In *From semiconductors to proteins: beyond the average structure*, Edited by S. J. L. Billinge and M. F. Thorpe, pp. 105, (Kluwer/Plenum, New York, 2002).
28. R. Osborn, E.A. Goremychkin, A.I. Kolesnikov, and D.G. Hinks, Phys. Rev. Lett. **87**, 017005 (2001).
29. I.-K. Jeong, Th. Proffen, F. Mohiuddin-Jacobs, and S.J.L. Billinge, J. Phys. Chem. A **103**, 921 (1999).
30. M. J. Graf, I. K. Jeong, D. L. Starr and R. H. Heffner, Phys. Rev. B **68**, 064305 (2003).
31. I.-K. Jeong, R.H. Heffner, M.J. Graf, and S. J. L. Billinge, Phys. Rev. B **67**, 104301 (2003).
32. C.H. Booth, F. Bridges, E.D. Bauer, G.G. Li, J.B. Boyce, T. Claeson, C.W. Chu, and Q. Xiong, Phys. Rev. B **52**, R15 745 (1995).
33. J.S. Chung and M.F. Thorpe, Phys. Rev. B **55**, 1545 (1997).